Static Aeroelastic Control of an Adaptive Wing

P.Gasbarri , F.Betti

Dipartimento Aerospaziale, Università di Roma "La Sapienza"

Via Eudossiana 18 - 00184 Roma, Italia

F.Persiani

Dipartimento delle Costruzioni Meccaniche Aeronautiche e Nucleari,

Universita' di Bologna, Italia

G.M. Saggiani

I.S.Aer.S, Forlì, Italia

Abstract

An examination on the ability of active material to improve the static aeroelastic performance of wings is investigated. A plate model with laminated composite skins is adopted for the wing box structure.

The box is rinforced with stringers modelled as spanwise placed axial elements that can incorporate piezoelectric actuators. The lifting surface formulation is used in order to evaluate the aerodynamical loads on the wing.

The ammount of wing performance improvement is constrained by limited electromechanical coupling coefficients and by the way active material is integrated into the main structure. These constraints are made less stringent by an active wing bay configuration in which axial piezoelectric actuators are discretely attached to the wing box skins. The numerical results reveal the ability of the adaptive wing to control the static aeroelastic response of unswept and swept-forward wing. Increase in divergence critical speed is proved and, in subcritical range, the power of adaptive control tecnique is shown in terms of elestic displacements and aerodynamic loads.

1 Introduction

Adaptive wings in which piezoelectric actuator layers are embedded in a laminated composite structure, show some limits [1] [2]:

i) they do not exploit the largest electromechanic piezoelectric coupling coefficient, that is in the direction of the poling direction, but the indirect effect in its orthogonal plane,due to the Poisson ratio, which is about the 30% of the largest one.

ii) practical available piezoelectric material are isotropic in the plane orthogonal to the poling direction, so that their authority on the twisting deformation mode is poor because it comes just from the bending-twisting coupling effect due to the anisotropic proprierties of the composite laminate and to the sweeep angle of the wing.

A different configuration is proposed in this work. The structural wing box is modelized as a plate structure made of orthotropic cover skins stiffned by spanwise placed stringers attached to the skins. The wing is made active by replacing the whole or some part of the stringers with axial piezoelectric actuators. This configuration overcomes both of the aforementioned limits, since it exploits the largest piezoelectric electro-mechanical coupling and, as it will be shown, it can directely induce twisting deformation on the wing improving the control authority.

Copyright © 1994 by ICAS and AIAA. All rights reserved.

2 Structural Model

A plate model is used to represent the wing box structure. The planform geometry of this plate model is assumed to be trapezoidal, with arbitrary sweep angle Λ with respect to the wind direction, and a nondimensional coordinate system (u, η) is adopted, as illustrated in Fig.(1). The wing box is assumed of uniform cross-section, altough the model is capable of modelling also non uniform one. The typical cross-section view of the analitical model is illustrated in Fig.(2).
The presence of ribs, insuring the transfer of shear stress between the upper and lower skins, is assumed in order to neglect the shear deformation of the cross-sections. The upper and lower skins are made of several layers that are assumed to have the same mechanical properties but different orientation. Furthermore the upper and lower skins and, hence, the corresponding layers are assumed to be symmetric about the middle plane of the wing. The anisotropic plate bending stiffness matrix $\mathbf{D}$ is evaluated by means of classical laminated theory. Stringers laying spanwise on $u = const$ lines and simmetrically placed with respect to the middle plane of the wing, are represented as axial elements discretely attached to the skins. Each segment between two connection points can be replaced with an axial active member as it will be discussed later.

A modified finite element method is used to obtain an approximately stationary solution to the variation of the total energy associated with the analytical model. This energy has the following expression:

$$\mathcal{E} = \mathcal{U} + \mathcal{V} - \mathcal{L} \tag{1}$$

where $\mathcal{U}$ is the strain energy of the strucure,$\mathcal{V}$ is the electromechanical coupling energy due to the active elements and $\mathcal{L}$ is the work done by the external loads.

2.1 Modified Finite Element Method

The modified finite element method used in this work [3], consists in assuming a spanwise finite element discretization of the wing elastic displacements, while a power expansion is assumed chordwise. These assumptions have the advantage to provide the analyst directly with global chordwise quantities such as flexural displacements, torsional rotations, mean line curvatures, etc. which are meaningfull from the aerodynamic standpoint. The general expression of the nondimensional flexural elastic displacement of the jth element is:

$$W_j(u,\zeta) = \frac{w_j(u,\zeta)}{L} = \mathbf{\Psi}^T(u,\zeta)\mathbf{X}_j \tag{2}$$

with

$$-0.5 \le u \le 0.5; \quad 0 \le \zeta \le 1 \tag{3}$$

where ζ, is the local nondimensional coordinate associated with each finite element. The function $\mathbf{\Psi}(u,\zeta)$ is the shape function vector and $\mathbf{X}_j$ is the vector of the generalized displacements of the jth element, their expression are given in Appendix A.

The strain energy of the jth wing plate element has the following expression:

$$\mathcal{U}_j = \frac{1}{2}\int_{S_j} \mathbf{k}_j^T(u,\eta)\mathbf{D}\mathbf{k}_j(u,\eta)dS \tag{4}$$

where $\mathbf{k}(u,\eta)$ is the plate curvature vector, that can be written in terms of the FEM generalized displacements in the form:

$$\mathbf{k}_j(u,\zeta) = \frac{1}{L}\mathbf{C}^T(u,\zeta)\mathbf{X}_j \tag{5}$$

the expression of the vector $\mathbf{C}(u,\zeta)$ is given in Appendix A. Substitution of the expression for the elastic displacements into the expression of the strain energy gives:

$$\mathcal{U}_j = \frac{1}{2}D_{11}\mathbf{X}_j^T\left(\beta\delta_j\int_0^1\int_{-0.5}^{+0.5}\mathbf{C}\mathbf{D}\mathbf{C}^T dud\zeta\right)\mathbf{X}_j \tag{6}$$

where $\mathbf{D} = D_{11}\hat{\mathbf{D}}$ and $\delta_j = L_j/L$. There are N_r couple of stringers simmetrically placed with respect to the middle plane along constant lines $u = u_r$ with $r = 1, N_r$. The stringers are represented as axial elements discretely attached to the upper and lower skins. The ends of each stringer finite element are in two adjacent attachment points. These points can be defined independentely with respect to the plate finite elements. The assumed nondimensional axial displacement of the kth element of the rth stringer has the expression:

$$U_k^r(\xi) = u_k(\xi)/L = \mathbf{N}^T(\xi)\mathbf{U}_k^r; \quad 0 \le \xi \le 1 \tag{7}$$

where ξ is the local non dimensional coordinate along the lenght of the stringers. The expression of the shape function vector $\mathbf{N}(\xi)$ and of the axial displacement vector $\mathbf{U}_k$ is given in Appendix A. The strain energy of the *kth* stringer element is:

$$\mathcal{U}_k^r = \frac{1}{2}\int_{l_k} \epsilon(\xi) EA \epsilon(\xi) dl \tag{8}$$

where $\epsilon(\xi)$ is the axial deformation. By imposing the condition that the end of the stringer element are constrained to the upper or lower skins, the axial displacements of the ends of the *kth* element $\mathbf{U}^r{}_k$ can be expressed in terms of the wing element generalized displacement vectors, as it is discussed in Appendix A, in the form:

$$\mathbf{U}_k^r = -\frac{h}{L}\Phi_k^r \begin{bmatrix} \mathbf{X}_{0k} \\ \mathbf{X}_{1k} \end{bmatrix} \tag{9}$$

In terms of the wing generalized displacements the strain energy of the *rth* couple of stringers, of Young modulus E and cross section area A, symmetrically placed with respect to the middle plane has the expression:

$$\mathcal{U}_k^r = D_{11}\left[\mathbf{X}_{0k}^T \mathbf{X}_{1k}^T\right]\left(\Gamma\beta\delta_k {\Phi_k^r}^T \int_0^1 \mathbf{S}\mathbf{S}^T d\xi\right)\Phi_k^r \begin{bmatrix} \mathbf{X}_{0k} \\ \mathbf{X}_{1k} \end{bmatrix} \tag{10}$$

where :

$$\Gamma = 2\frac{EAh^2}{cD_{11}} \tag{11}$$

$$\delta_k = \frac{l_k}{L} \tag{12}$$

Summing up the strain energy of all the plate elements and the stringer elements, the global strain energy can be written in the form:

$$\mathcal{U} = D_{11}\left[\frac{1}{2}\mathbf{X}^T\left(\mathbf{K}_p + \sum_{r=1}^{Nr}\mathbf{K}_s^r\right)\mathbf{X}\right] \tag{13}$$

where N_r is the number of the couple of the stringers symmetrically placed with respect to the middle plane, $\mathbf{X}$ is the vector of the global degree of freedom, $\mathbf{K}_p$ and $\mathbf{K}_s$ are the stiffner matrices of the plate and stringers respectively, assembled accordingly to classical FEM method.

2.2 Actuator Wing Bay

The actuators are symmetrically placed with respect to the middle plane. When one of the element of a stringer is replaced by an axial piezoelectric actuator the electro-mechanical coupling energy should be taken into account. For such an active element:

$$\mathcal{U}_k^r + \mathcal{V}_k^r = \frac{1}{2}\int_{l_k} \epsilon EA(\epsilon - \Lambda_k) dl \tag{14}$$

in which Λ_k is the actuator strain. For piezoelectric actuators the constitutive equation gives:

$$\Lambda = d_{33} E_3$$

where the subscript 3 indicate the poling direction, d_{33} is the electro-mechanical coupling coefficent and E_3 is the electric applied field. Each couple of actuators, symmetrically placed with respect to the middle plane, are connected in such a way that they induce an out-of-phase strain in the upper and lower skins, thus no net in-plane strain is induced on the wing:

$$\Lambda_{upper} = \Lambda$$

$$\Lambda_{lower} = -\Lambda$$

In term of the generalized displacements of the wing, $\mathcal{U}_k^r$ has the same expression as Eq.(13) while the term $\mathcal{V}_k^r$ can be written:

$$\mathcal{V}_k^r = -D_{11}\left[\left[\mathbf{X}_{0j}^T \mathbf{X}_{1j}^T\right]\left(\Gamma_A\beta\delta_k {\Phi_k^r}^T \int_0^1 \mathbf{S} d\xi\right)\hat{\Lambda}_k\right] \tag{15}$$

with:

$$\hat{\Lambda} = \Lambda/\Lambda_{max} \tag{16}$$

$$\Gamma_A = 2\frac{EAh}{\beta D_{11}}\Lambda_{max} \tag{17}$$

where Λ_{max} is the maximum free induced strain and Λ is the actuator strain. The wing active bay is obtained by placing the active elements symmetrically with respect to the wing planform center line, along the constant lines $u = \pm u_r$, as it is shown in Fig.(4). For a straight isotropic wing, when each couple of chordwise symmetric actuators are connected out-of-phase, pure twisting deformation is induced on the wing, while, when they are connected in-phase, a deformation of pure bending arises. Any combination of these two actuation modes can be obtained by independently driving each actuators. However, for each active wing bay, the skew-symmetric

part of the actuator strain gives a contribution to the wisting mode, while the symmetric part gives a contribution to the bending mode. For the sake of clearness, hese two contribution are evaluated separately. It will e referred to as twisting and bending actuator bay when he skew-symmetric and symmetric actuation are considered respectively, and the subscripts t and b will be used. Thus the electromechanical coupling energy of the kth ctive bay has the expression:

$$\mathcal{V}_k = -D_{11}\left[\mathbf{X}_k^T(\mathbf{P}_{b,k}\Lambda_{b,k} + \mathbf{P}_{t,k}\Lambda_{t,k})\right] \tag{18}$$

vith:

$$\begin{aligned}\mathbf{P}_{t,k} &= \Gamma_A\beta\delta_k(\Phi_k^{r\,T} - \Phi_k^{-r\,T})\int_0^1 \mathbf{S}d\xi \\ \mathbf{P}_{b,k} &= \Gamma_A\beta\delta_k(\Phi_k^{r\,T} + \Phi_k^{-r\,T})\int_0^1 \mathbf{S}d\xi\end{aligned} \tag{19}$$

nd

$$\begin{aligned}\Lambda_{b,k} &= \Lambda_k^r + \Lambda_k^{-r} \\ \Lambda_{t,k} &= \Lambda_k^r - \Lambda_k^{-r}\end{aligned} \tag{20}$$

where the superscript $\pm r$ are used to indicate quantities valuated for $u = \pm u_r$. The electric connections of the iezoelectric actuator bay are sketched in Fig.(4).

This expression of $\mathcal{V}_k$ can be assembled according to EM rule in order to obtain global expression for the oupling energy in terms of the vector of the wing generalized displacements:

$$\mathcal{V} = -D_{11}\left[\mathbf{X}^T(\mathbf{P}_b\mathbf{\Lambda}_b + \mathbf{P}_t\mathbf{\Lambda}_t)\right] \tag{21}$$

where the vectors $\mathbf{\Lambda}_b$ and $\mathbf{\Lambda}_t$ are the vectors of the symmetric and skew-symmetric strain applied to each active bay. For wings with anisotropic skins or sweep angle bending-twisting coupling arises, however actuation of the active wing can be tuned in order to obtain the esidered actuation mode. From Eqs.(13) and (18), the tationary solution of the variation of the total energy ives the governing equation of the active wing:

$$\mathbf{K}_{na}\mathbf{X} = \mathbf{P}_b\mathbf{\Lambda}_b + \mathbf{P}_t\mathbf{\Lambda}_t + \mathbf{F}_{ext} \tag{22}$$

where:

$$\mathbf{K}_{na} = \mathbf{K}_p + \sum_{s=1}^{N_r}\mathbf{K}_s^r \tag{23}$$

is the non-active stiffness matrix.

2.3 Adaptive Wing

The wing is now active but not adaptive. The adaptive nature of the wing is introduced by requiring the piezoelectric applied strain to be related to the actual deformation of the wing. Based on the converse piezoelectric effect, a sensor bay with the same configuration as the active bay is placed close to the wing root in order to pick up the twisting and bending deformation. For static application the charge q, caused by the wing deformation, is collected on the electrodes placed on the basis of the piesoelectric material and measured by a charge amplifier. The sensing equation of an axial piezoelctric sensor of lenght l is:

$$q = d_{33}\frac{EA}{l}\int \epsilon dl \tag{24}$$

Twisting and bending sensor bays are obtained by connecting the piezoelectric elements in the same manner as for the actuator bays . In terms of the generalized displacements the charge measured on the electrodes of the sensor bay and due to the bending and twisting deformations are respectively:

$$q_b = \frac{d_{33}}{\Lambda_{max}l}P_{b,s}^T\begin{bmatrix}X_{0s}\\X_{1s}\end{bmatrix} \tag{25}$$

$$q_t = \frac{d_{33}}{\Lambda_{max}l}P_{t,s}^T\begin{bmatrix}X_{0s}\\X_{1s}\end{bmatrix} \tag{26}$$

where the subscript s indicates the sensor bay.

The adaptive nature of the wing is introduced by requiring that the actuator strain of the kth actuator bay be proportional to the deformation measured by the sensor bay. The result is:

$$\Lambda_{b,k} = g_bP_{b,s}^T\begin{bmatrix}X_{0s}\\X_{1s}\end{bmatrix} \tag{27}$$

$$\Lambda_{t,k} = g_tP_{t,s}^T\begin{bmatrix}X_{0s}\\X_{1s}\end{bmatrix} \tag{28}$$

Substituting Eqs.(27) and (28) in Eq.(22) and assembling, we obtain the matrix form of the governing equation of the adaptive wing:

$$(\mathbf{K}_{na} + g_b\mathbf{K}_b + g_t\mathbf{K}_t)\,\mathbf{X} = \mathbf{F}_{ext} \qquad (29)$$

where $\mathbf{K}_b$ and $\mathbf{K}_t$ are the feed-back matrix of the flexural and twisting control respectively and g_b and g_t are the relevant gains.

3 Aerodynamic Model

For the present research, it is necessary to have an aerodynamic tool that can adequately describe the aerodynamic steady load acting on the wing, in subsonic uncompressible flow. One of the most popular method, that can be used to determine aerodynamic forces, is the Kernel-Function-Method. Which is able to characterize the aerodynamic pressure in some wing colocated points. One of the major advantages of the KFM is that few colocated points are able to well describe the pressure distribution on the wing, so that few aerodynamic degrees of freedom are needed [4] [5] [6].

3.1 Review of Kernel-Function-Method

The fundamental equation of KFM is an integral one. This equation relates load distribution to normalwash. In steady flow we have the following expression:

$$\frac{w(x,y)}{U_\infty} = -\frac{1}{8\pi q_{dyn}} \oint\!\!\!\!\!\!\int_S \Delta p(\bar{x},\bar{y}) G(x,y,\bar{x},\bar{y})\, d\bar{x}\, d\bar{y} \qquad (30)$$

where (x,y) and $(\bar{x},\bar{y})$ are control point and doublet singularity point respectively, $\oint\!\!\!\!\!\!\int_S$ signifies the treatment of improper integral according Hadamard rule,$G(x,y,\bar{x},\bar{y})$ is the kernel of the integral equation (App.B) and q_{dyn} is the dynamic pressure.

The idea of KFM is to approximate the unknowm pressure distribution $\Delta p(\bar{x},\bar{y})$ in chordwise and spanwise directions by prescribed functions with unknown coefficients $q_{\mu\nu}$. In order to obtain a most accurate solution, these funtions must take into account the Kutta conditions of zero pressure at the trailing edge and square root singularity at the leading edge of the wing, while along spanwise they can be selected according the well known Multhopp rule. In nondimensional variables we have:

$$\Delta P(\bar{u},\bar{\eta}) = \sum_\mu \sum_\nu q_{\mu\nu}\varphi_\mu(\bar{u})\psi_\nu(\bar{\eta})\sqrt{\frac{1-\bar{u}}{\bar{u}}} \qquad (31)$$

where:

$$\begin{aligned} \bar{\eta} &= \frac{y}{L} \\ \bar{u}(x,y) &= \frac{x - x'(y)}{c(y)} \end{aligned} \qquad (32)$$

with L the lenght of wing semispan, x the abscissa along chord direction, $x'(y)$ the leading edge equation and $c(y)$ the chord lenght at the coordinate y. The function $\varphi_\mu(u)$ represent the Lagrange polynomial of unity strenght at the μ-th control point along chord direction:

$$\varphi_\mu(\bar{u}) = \sum_{r=0}^{M-1} C_{\mu r}\bar{u}^r \qquad (33)$$

Where the coefficents $C_{\mu r}$ can be determined solving the following alebraic system:

$$\mathbf{CV} = \mathbf{I} \qquad (34)$$

with $\mathbf{V}$ Vandermonde matrix, written for all the control points and $\mathbf{I}$ is the unit matrix. The expression of Multhopp function $\psi_\nu(\bar{\eta})$ is:

$$\psi_\nu(\bar{\eta}) = \frac{2}{N+1}\sum_{s=1}^{N} \sin(s\theta_\nu)\sin(s\theta) \qquad (35)$$

with:

$$\theta = \arccos(\bar{\eta}) \qquad 0 \le \theta \le \pi \qquad (36)$$

and θ_ν the control point coordinate according the well known Multhopp rule:

$$\theta_\nu = \frac{\pi}{N+1}\nu \qquad \nu = 1,\ldots,N \qquad (37)$$

By solving the singular integral equation (30) we obtain an algebraic equation in terms of unknown nondiomensional pressure vector $\mathbf{q}$:

$$\mathbf{Aq} = \alpha_g + \alpha_e \qquad (38)$$

where α_g and α_e are the vectors of the geometric and elastic incidence in the aerodynamic control points.

4 Static Aeroelasticity

In order to valuate the static divergence of the wing it is necessary to relate external aerodynamic loads to elastic displacements. Starting from the work performed by aerodynamic forces, it is possible to find the relationship between aerodynamic and structure. The work performed by the generalized aerodynamic forces on the generalized displacements of the jth wing element is:

$$\mathcal{L}_j = \int_{S_j} w_j(x,y) F_j(x,y) dxdy \tag{39}$$

Taking into account the following relationship between the structural and aerodynamic coordinate of the jth element:

$$\begin{aligned} \bar{u} &= u + 0.5; \qquad -1/2 \le u \le 1/2 \\ \bar{\eta} &= \bar{\eta}_j + \zeta \delta_j; \qquad 0 \le \zeta \le 1 \end{aligned}$$

the aerodynamic load on the jth element is:

$$F_j(u,\zeta) = q_{dyn} \mathbf{Q}^T(u,\zeta)\mathbf{q} \tag{40}$$

where $\mathbf{Q}(u,\zeta)$ is the aerodynamic shape function vector, whose expression is given in Appendix B.

By putting Eq.(2) and Eq.(40) into Eq.(39) and using nondimensional variables we obtain for the work of the jth element:

$$\mathcal{L}_j = \sigma D_{11} \mathbf{X}_j^T \mathbf{R}_j \mathbf{q} \tag{41}$$

with:

$$\mathbf{R}_j = L_j \int_0^1 \int_{-0.5}^{0.5} \Psi(u,\zeta) \mathbf{Q}^T(u,\zeta) du d\zeta \tag{42}$$

and σ is the nondimensional dynamic pressure:

$$\sigma = \frac{cL^2}{D_{11}} q_{dyn} \tag{43}$$

Finally the aerodynamic force on the wing finite element is:

$$\mathbf{F}_j = D_{11} \sigma \mathbf{R}_j \mathbf{q} \tag{44}$$

which, assembled for the whole wing, gives us the global force vector:

$$\mathbf{F}_{ext} = D_{11} \sigma \mathbf{R} \mathbf{q} \tag{45}$$

The ith element of the vector of the elastic incidence is:

$$\alpha_{e,i} = \alpha_e(u_i, \eta_i) = \frac{1}{\beta} \frac{\partial}{\partial u} W(u,\eta) \mid_{u_i,\eta_i}$$

by performing simple algebra this vector can be expressed in terms of generalized displacement of the FEM as:

$$\alpha_e = \mathbf{T}\mathbf{X} \tag{46}$$

Combining Eqs.(17,38,45,46) we obtain the final aeroelastic equation which allows to determine the unknown vector $\mathbf{q}$:

$$\left(\mathbf{A} - \sigma \mathbf{T} \mathbf{K}^{-1} \mathbf{R}\right) \mathbf{q} = \alpha_g \tag{47}$$

where $\mathbf{K}$ is the global stiffness matrix of the adaptive wing:

$$\mathbf{K} = \mathbf{K}_{na} + g_b \mathbf{K}_b + g_t \mathbf{K}_t \tag{48}$$

From this equation the vector of the aerodynamic load on the wing $\mathbf{q}$ can be evaluated as a function of the geometric incidence α_g, taking into account the elastic displacements. The divergence non dimensional dynamic pressure σ is given by the lowest eigenvalue of the following algebraic equation:

$$det(\mathbf{A} - \sigma \mathbf{T} \mathbf{K}^{-1} \mathbf{R}) = 0 \tag{49}$$

5 Numerical Results

For the purpouse of the numerical verification, a wing with the geometric and mechanic properties of Table 1 is considered. Four stringer are symmetrically placed with respect to the center line of the wing along the constant lines $u = \pm 0.25$, on the upper and lower skins. Three terms are used in the chordwise power expansion of the wing displacement shape functions and 15 spanwise elements are used to represent the FEM discretization. Each actuator bay is assumed coincident with a finite element, while the sensor bay is placed in the element closest to the wing root.

As a first step the actuation capabilities of the active wing are investigated. The unswept and forward-swept wings with sweep angles of $0°$,$-30°$ and $-60°$ are considered. All the bays are actuated by inducing the the maximum actuator strain. The effects of the deformation due to the bending and twisting mode actuation are considered separately. Figs.(5),(6) and (7) show the effect of twisting actuator bays on the wing. For the unswept wing, Fig.(5), pure twisting deformation arises, while the bending-twisting coupled deformation increases with the

sweep angle. Figs.(6) and (7) show a progressive decrease of the authority of twisting mode actuation in controlling the twisting deformation of the wing. The effect of the bending actuator bay is showed for the sweep angles $0°$,$-30°$ and $-60°$ in Figs.(8),(9) and (10). Conversly with respect to the twisting actuator bay, pure bending deformation arises on the unswept wing, while progressively larger twisting deformations appear increasing the sweep angle.

Figs.(11) and (12) show the variation of the divergence critical speed of the adaptive wing versus the feedback gain of bending and twisting actuator bays respectively. The critical speed contour is shown for two differnt sweep angles that are $-30°$ and $-60°$.

In Figs.(13) and (14) is displaied a paramaetric study on the best placement of one bending and one twisting actuator bay bay, in order to accomplish the largest divergence speed. For the sweep angle of $-30°$, Fig.(13), the higest divergence speed is obtained when the twisting and bending mode actuator bays are placed in the elements 5 and 6 of FEM modellization, while it occurs when they move through the wing tip, in the element 7 for both bending and twisting actuator bay, for the sweep angle $-60°$, Fig.(14).

Figs.(15),(16),(21),(22) display the response and the aerodynamic loads of the non-adaptive wing of sweep angles $-30°$ and $-60°$, corresponding to a dynamic pressure $q_{dyn} = 0.8q_D$, where q_D is divergence dynamic pressure. The same quantities are displaied in Figs. (17), (18), (19), (20), (23), (24), (25), (26) for the adaptive wing for which one twisting and one bending active bays are placed according to the best locations given by the parametric study of Figs. (13) and (14).

Figs.(11) and (12) show a significative increase in the divergence speed that can be accomplished by such an adaptive wing. From the aeroelastic stand point high autority on twisting deformation is desired, while attenuation of bending deformation are requested by material strenght.

Comparison between Figs.(10) and (11) shows that the divergence speed is governed mainly by twisting deformation, as a consequence, due to the geometrical coupling, the autority of bending actuator bay on the critical speed increase with the sweep angle, while the twisting actuator bay is more effective for small sweep angle. A combination of this two deformation modes is not investigated, however it is reasonable to expect that it would be lead to better performances and allow the designer to tune more adequately the control system.

Below the critical speed the power of the adaptive wing is revealed by the positive effect of the attenuation of the elastic deformation on the aerodynamic load distribution.

It should be noted that in this study the issue associated with power consumption and actuator saturation has not be addressed.

6 Conclusion

A laminated composite plate reinforced with stringers, part of which are made of piezoelectric material, has been used to model wing box structure of an adaptive wing. The study of the aeroelstic behaviour of the wing has been accomplished.

Piezoelectric axial actuators are used to exploit the largest electromechanical coupling coefficient and to make possible pure twisting deformation. A configuration of the wing active bay needed in order to induce bending and twisting mode deformation on the wing is proposed.

The effects of bending and twisting mode attenuation are examinated separately in terms of divergence speed increase and, in the subcritical range, in terms of wing deformation and aerodynamic load distribution.

The obtained results reveal the great potential of such an adaptive wing to increase the divergence critical speed and they show the high control autority of twisting active bay for low wing seep angle, while bending active bay are more efficient, due to geometrical coupling, for high wing seep angle.

A parametric study for the best placement of twisting and bending active bay of swept-forward wing is accomplished and the results applied to the adaptive wing. They reveal the ability of the adaptive wing to control lift distribution by attenuating elastic displacements.

7 Aknowledgments

The Authors are very grateful to Prof. Paolo Santini for the suggestions received and for the stimulating discussions had with him during the preparation of this work.

A Appendix

A local coordinate is introduced for each spanwise element of the wing of lenght L_j:

$$\zeta = \frac{\eta - \eta_j}{\delta_j}; \quad 0 \leq \zeta \leq 1 \tag{50}$$

where η_j is the initial coordinate of the finite element in the wing global coordinate system and $\delta_j = L_j/L$ the nondimensional lenght of the finite element.

The elastic flexural displacement of the wing element is:

$$w_j(u,\zeta) = \frac{w_j(u,\zeta)}{L} = \Psi^T(u,\zeta)X_j \tag{51}$$

for shape function vector $\Psi^T(u,\zeta)$ the following expression has been used:

$$\begin{aligned}\Psi^T(u,\zeta) \quad &= \left[\psi_1, \psi_2, \beta u\psi_1, \beta u\psi_2, \ldots, (\beta u)^{N-1}\psi_1, (\beta u)^{N-1}\psi_2 \mid \right. \\ &\left. \psi_3, \psi_4, \beta u\psi_3, \beta u\psi_4, \ldots (\beta u)^{N-1}\psi_3, (\beta u)^{N-1}\psi_4\right] \end{aligned} \tag{52}$$

where $\beta = c/L$ and the functions $\psi_j = \psi_j(\zeta)$ are the classical FEM shape functions for a beam:

$$\begin{aligned}\psi_1(\zeta) &= 1 - 3\zeta^2 + 2\zeta^3 \\ \psi_2(\zeta) &= \zeta(1 - 2\zeta + \zeta^2)L_j \\ \psi_3(\zeta) &= -3\zeta^2 r - 2\zeta^3 \\ \psi_4(\zeta) &= (-\zeta^2 + \zeta^3)L_j \end{aligned} \tag{53}$$

As a consequence the genaralized displacement vector of the jth finite element is:

$$\begin{aligned}\mathbf{X}_j^T = &[(W_0 W_0' W_1 W_1', \ldots, W_{N-1} W_{N-1}')_0 \\ &(W_0 W_0' W_1 W_1', \ldots, W_{N-1} W_{N-1}')_1] \end{aligned} \tag{54}$$

where the subscripts 0 and 1 are used for the genarilezed displacemets defined on the left and right side of the finite element respectively. In the numerical examples presented in this paper it has been set $N = 3$.

In terms of the FEM generalized displacements defined above, the curvature vector $\mathbf{k}_j(u,\zeta)$ of the jth element has the expression:

$$\mathbf{k}_j(u,\zeta) = \frac{1}{L}\mathbf{C}^T(u,\zeta)\mathbf{X}_j \tag{55}$$

where:

$$\begin{aligned}\mathbf{C}^T(u,\zeta) \quad = \quad &\frac{1}{\beta^2}\begin{bmatrix} -1 \\ -\vartheta^2 \\ 2\vartheta \end{bmatrix}\Psi^T_{,uu}(u,\zeta) + \frac{1}{\delta_j^2}\begin{bmatrix} 0 \\ -1 \\ 0 \end{bmatrix}\Psi^T_{,\zeta\zeta}(u,\zeta) + \\ &\frac{1}{\delta_j\beta}\begin{bmatrix} 0 \\ 2\vartheta \\ -2 \end{bmatrix}\Psi^T_{,u\zeta}(u,\zeta) \end{aligned} \tag{56}$$

in which $\vartheta = \tan\Lambda$.

Concerning the discretely attached stringer placed spanwise along the constant line $u = u_r$, each element of the stringer is defined between two adjacent attachment points. The local coordinate along each element of lenght l_k is defined as:

$$\xi = \frac{s - s_k}{\delta_k}; \quad 0 \leq \xi \leq 1 \tag{57}$$

where s_k is the initial coordinate of the finite element in the stringer global coordinate systems and δ_k is the finite element lenght. The kth elastic extensional displacement of the rth stringer element is

$$U_k^r(\xi) = \frac{u_k(\xi)}{L} = \mathbf{N}^T(\xi)\mathbf{U}_k^r \tag{58}$$

where the shape function vector has the following expression:

$$\mathbf{N}^T(\xi) = [(1 - \xi), \xi] \tag{59}$$

and $\mathbf{U}_k^r$ are the extensional displacements of the ends of the elements. As a consequence the extensional strain is:

$$\epsilon_k = \frac{\partial u}{\partial s} = \mathbf{S}^T(\xi)\mathbf{U}_k^r \tag{60}$$

with

$$\mathbf{S}(\xi) = \frac{1}{\delta_k}\mathbf{N}'(\xi)$$

The constrain that the ends of the elements are attached to the wing box skins, are imposed by expressing the stringer displacement vector $\mathbf{U}_k^r = \{U_{k0}^r, U^r{}_{k1}\}$ in term of the wing generalized displacements. By using the subscript 0 and 1 for the wing elements where the two ends

of the stringer element are attached respectively, we have the the following constrain:

$$\mathbf{U}_k^r = -\frac{h}{L}\Phi_k^r \begin{bmatrix} \mathbf{X}_{0k} \\ \mathbf{X}_{1k} \end{bmatrix} \tag{61}$$

where

$$\Phi_k^r = \begin{bmatrix} \Psi_{,\zeta}\,|_{u=u_r,\zeta=\zeta_0} & 0 \\ 0 & \Psi_{,\zeta}\,|_{u=u_r,\zeta=\zeta_1} \end{bmatrix} \frac{\cos\Lambda}{\delta_k} \tag{62}$$

and h is the height of the stringer from the middle plane.

B Appendix

Kernel of steady aerodynamic:

$$G = \left[1 + \frac{x-\bar{x}}{\sqrt{(x-\bar{x})^2 + \beta^2\left[(y-\bar{y})^2 + z^2\right]}}\right] \frac{1}{(y-\bar{y})^2} \tag{63}$$

where $\beta = \sqrt{1-M_\infty^2}$ and M_∞ is Mach number; while the coordinates $(\bar{x},\ \bar{y})$ and $(x,\ y)$ represent the location of singularity point and the colocation point respectively.

The aerodynamic shape function has the following expression in nondimensional coordinate:

$$\begin{aligned}\mathbf{Q}^T(\bar{u},\bar{\eta}) \;=\; & [\psi_1\varphi_1, \psi_1\varphi_2, \ldots, \psi_1\varphi_{N_a}, \\ & \ldots, \psi_{M_a}\varphi_1, \psi_{M_a}\varphi_2, \ldots, \psi_{M_a}\varphi_{N_a}]\end{aligned} \tag{64}$$

where $N_a M_a$ is the number of the aerodynamic degree of freedom and the expression of the functions $\varphi_j = \varphi_j(\bar{u})$ and $\psi_j = \psi_j(\bar{\eta})$ are given in Sec. 3.1 of the main text.

References

[1] CRAWLEY E.F., LAZARUS K.B., *"Induced Strain Actuation of Isotropic and Anisotropic Plates*, AIAA Journal, Vol.29, No.6, 1989.

[2] S.M. EHLERS, T.A. WEISSHAAR," *Static Aeroelastic Con trol of an Adaptive Lifting Surface*, Journal of Aircraft Vol.30,No.4 Jul-Aug. 1993

[3] P. SANTINI, M. A. SNEIDER, L. LEUZZI, "Structural dynamic of a cantiliver sweep wing ", *L'Aerotecnica Missili e Spazio*, September 1986, pp. 141-149

[4] P. SANTINI, " *A general computer program for the calculation of the generalized aerodynamic forces"*. Presented at 47-th Meating of SMP AGARD, Florence,Italy, September 1978.

[5] P. SANTINI,P. GASBARRI,C.COPPOLA , *"Gli effetti di spessore nella valutazione della distribuzione delle pressioni sulla superficie del timone"*. Università degli Studi di Roma "La Sapienza" and I.N.S.E.A.N. RT cod.243/R, in italian, 1990.

[6] P. SANTINI,P. GASBARRI , *"Unsteady Aerodynamic In Subsonic Regimes* to be published.

[7] O.SONG, L.LIBRESCU, C.A. ROGERS," *Application of Adaptive Technology to Static Aereolastic Control of Wing Structures"*, AIAA Jo urnal, Vol.30,No.12, December 1992.

[8] P. SANTINI,F. BETTI, P.GASBARRI, A.ROSSI " *Actively Damped Piezoelectric Composite Wing"* . Presented at Damping '9 3, February 24-26,1993, San Fracisco, CA.

[9] P. SANTINI, *"Costruzioni Aeronautiche"*. E.S.A (198 6)

Semispan, L	$12m$
Chord, c	$2m$
Box Thickness	$20cm$
No. of Plys	4
Skin Thickness	$2mm$
Ply Orientation	$[90_2/0_2]$
α_g	3°
E_{11}	$103GPa$
E_{22}	$181GPa$
ν_{12}	0.28
ν_{21}	0.016
G_{12}	$7.17GPa$
E, Stringer	$70Gpa$
A, Stringer	$70mm^2$
Λ_{max}, Stringer	$300\mu strain$

Table 1: Geometrical and Mechanical Properties of the Wing

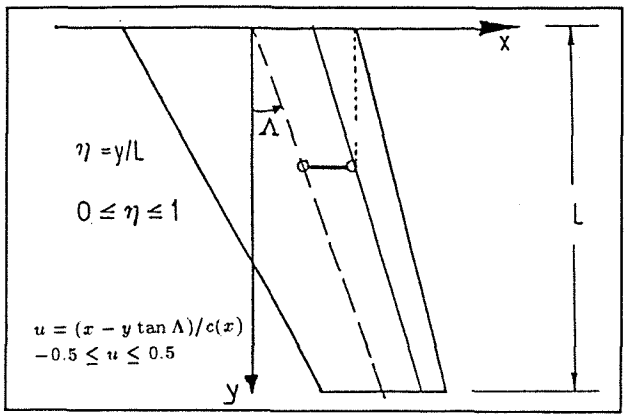

Figure 1: Non dimensional coordinates and reference frame

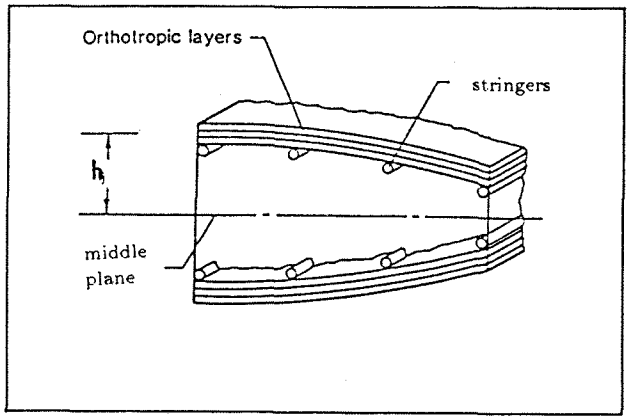

Figure 2: Wing box section

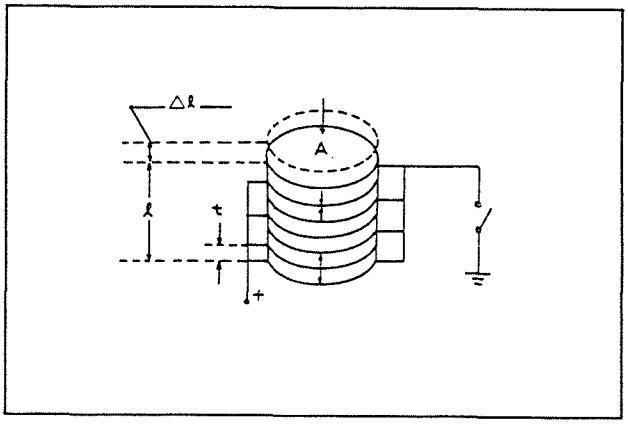

Figure 3: Axial Piezoelectric Actuator

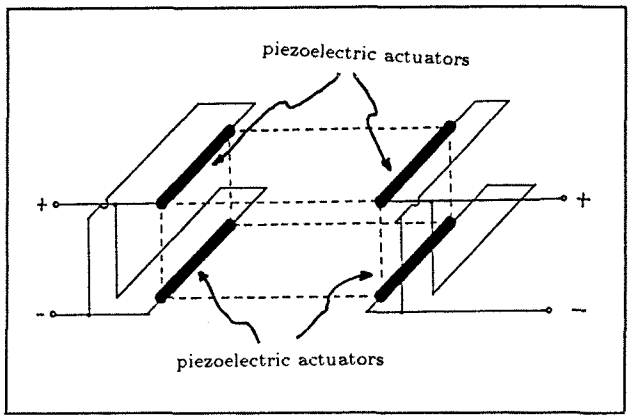

Figure 4: Actuator Bay Configuration

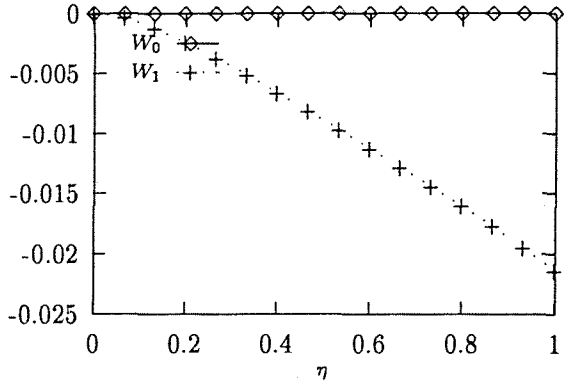

Figure 5: Center Line and Rotation Response to Torsional Activated Actuators $\Lambda = 0$

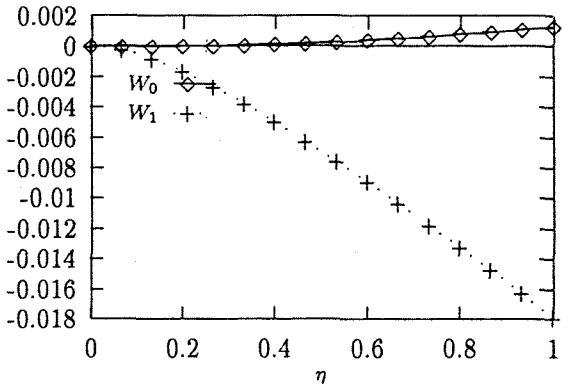

Figure 6: Center Line and Rotation Response to Torsional Activated Actuators $\Lambda = -30$

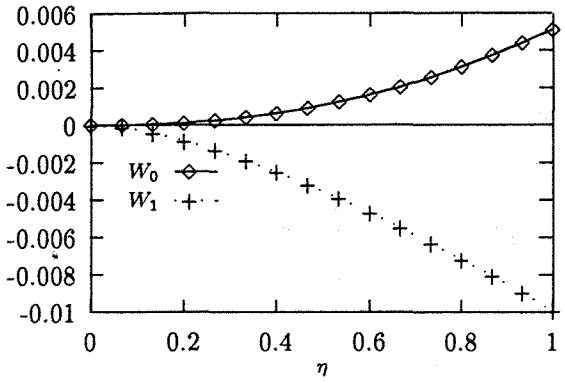

Figure 7: Center Line and Rotation Response to Torsional Activated Actuators $\Lambda = -60$

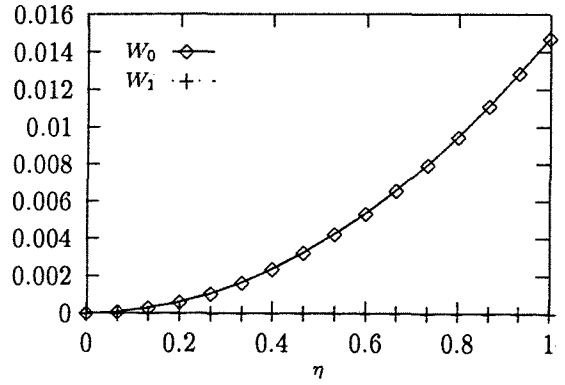

Figure 8: Center Line and Rotation Response to Flexural Activated Actuators $\Lambda = 0$

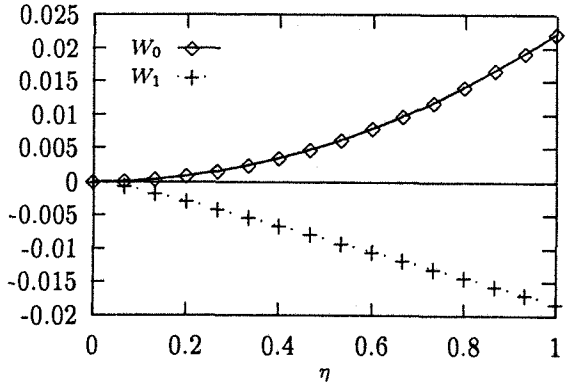

Figure 9: Center Line and Rotation Response to Flexural Activated Actuators $\Lambda = -30$

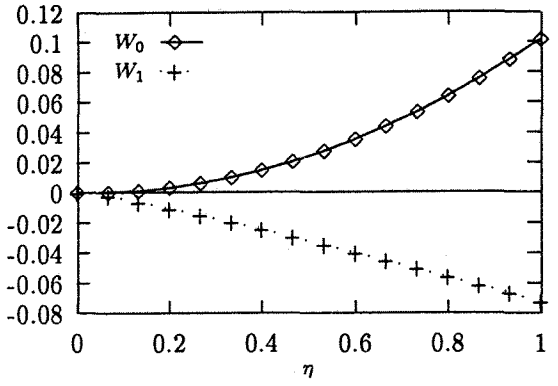

Figure 10: Center Line and Rotation Response to Flexural Activated Actuators $\Lambda = -60$

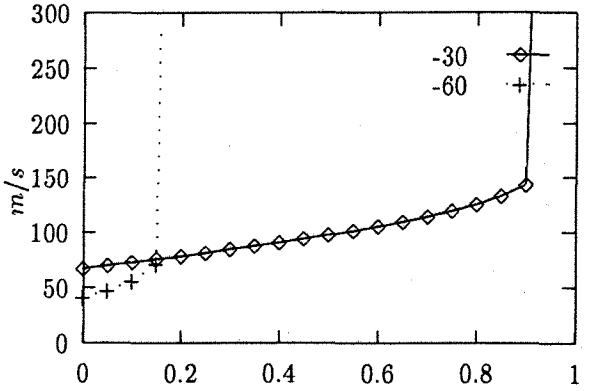

Figure 11: Divergence speed vs feed-back gain of bending actuator bays g_b for two sweep angle wing configurations

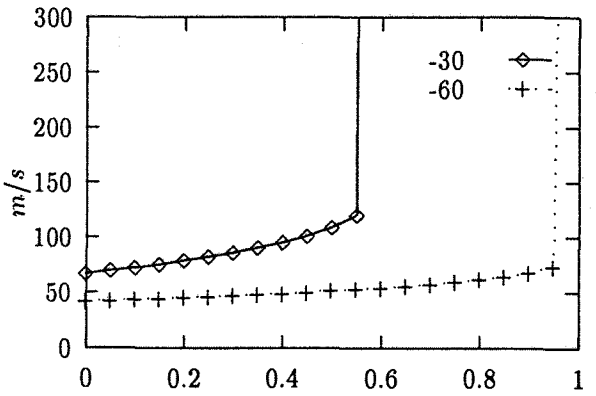

Figure 12: Divergence speed vs feed-back gain of twisting actuator bays g_t for two sweep angle wing configurations

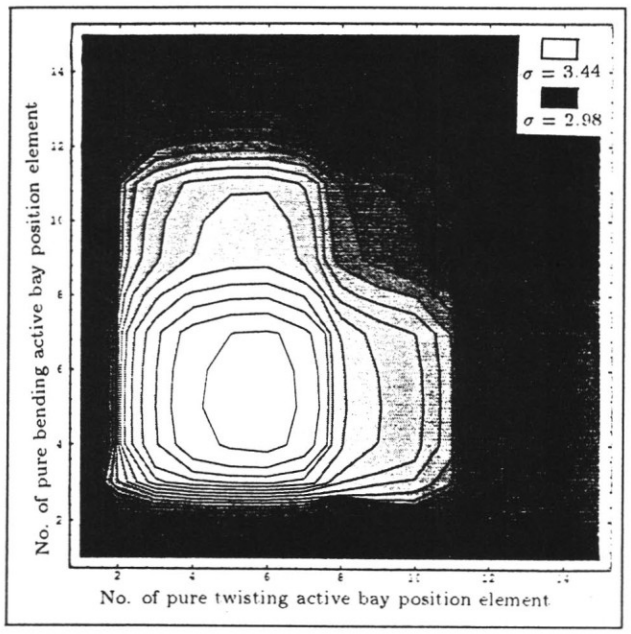

Figure 13: Isoline of σ_{cr} vs the position of one bending and one twisting active bay, $\Lambda = -30°$

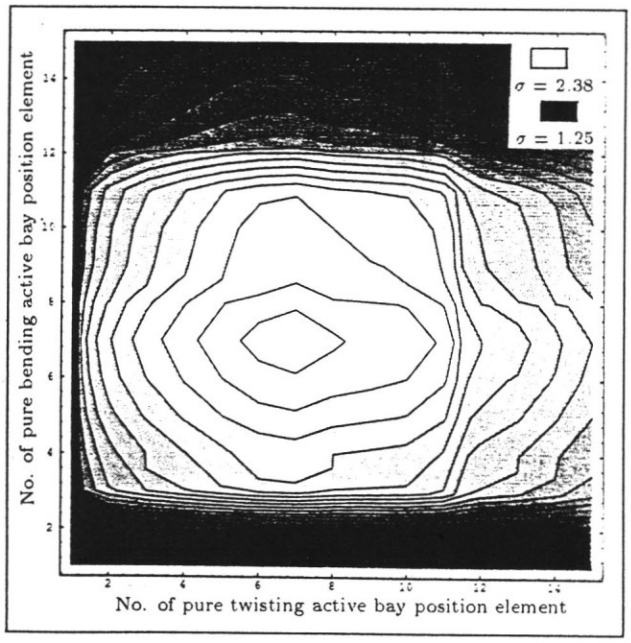

Figure 14: Isoline of σ_{cr} vs the position of one bending and one twisting active bay, $\Lambda = -60°$

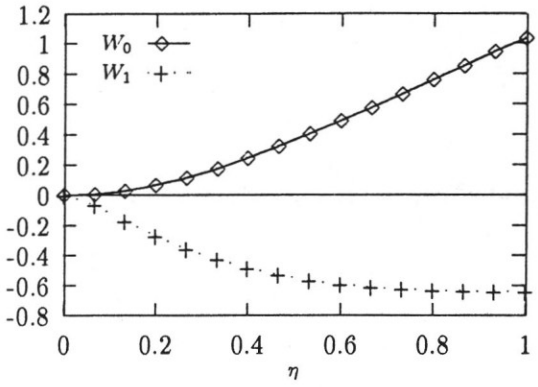

Figure 15: Center Line and Rotation Elastic Response to the Aerodynamic Load with $g_f = 0$ and $g_t = 0$ for $\Lambda = -30°$.

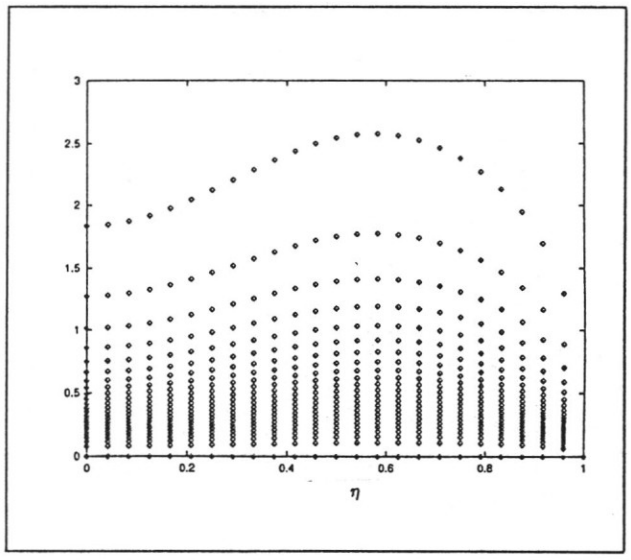

Figure 16: Spanwise Aerodynamic Load Distribution with $g_f = 0$ and $g_t = 0$. for $\Lambda = -30°$

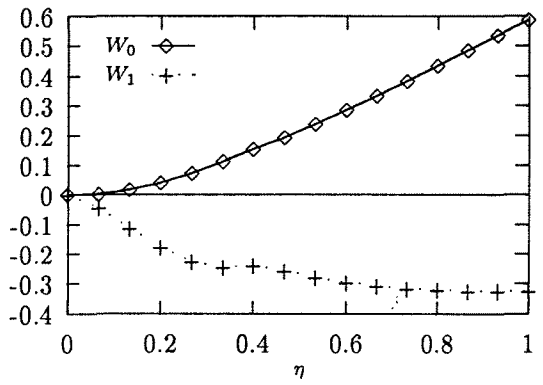

Figure 17: Center Line and Rotation Elastic Response to the Aerodynamic Load with $g_f = 0.5$ and $g_t = 0.5$ for $\Lambda = -30°$.

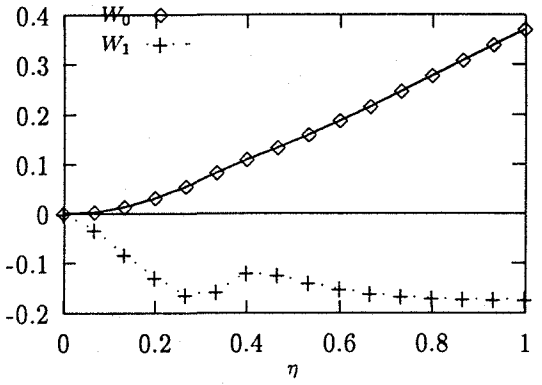

Figure 19: Center Line and Rotation Elastic Response to the Aerodynamic Load with $g_f = 1.$ and $g_t = 1.$ for $\Lambda = -30o$.

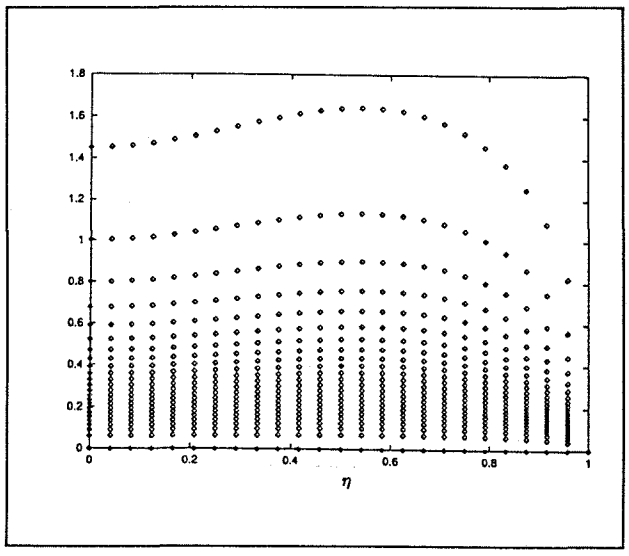

Figure 18: Spanwise Aerodynamic Load Distribution with $g_f = 0.5$ and $g_t = 0.5$ for $\Lambda = -30°$

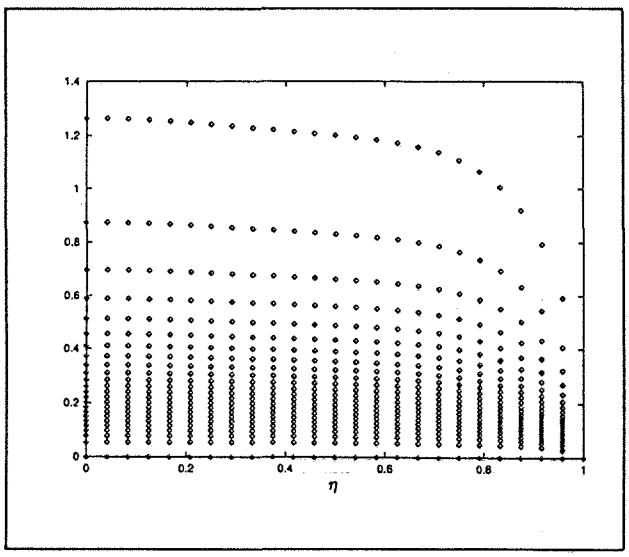

Figure 20: Spanwise Aerodynamic Load Distribution with $g_f = 1.$ and $g_t = 1.$ for $\Lambda = -30°$

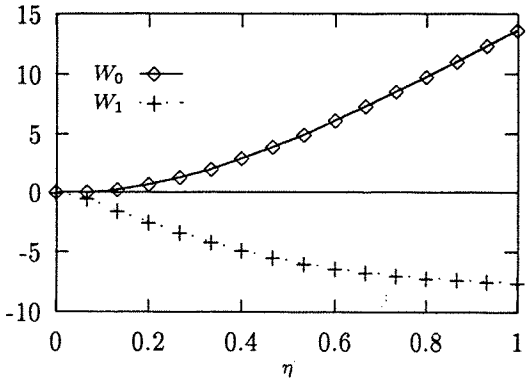

Figure 21: Center Line and Rotation Elastic Response to the Aerodynamic Load with $g_f = 0.$ and $g_t = 0.$ for $\Lambda = -30°$.

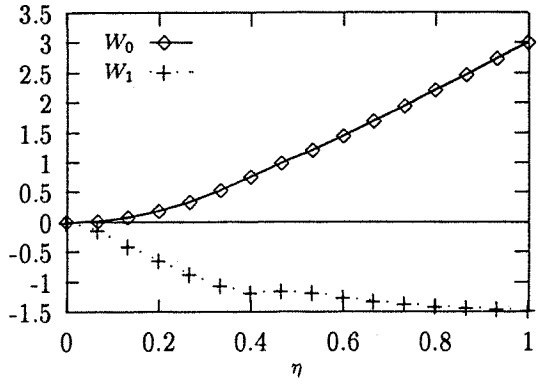

Figure 23: Center Line and Rotation Elastic Response to the Aerodynamic Load with $g_f = 0.5$ and $g_t = 0.5$ for $\Lambda = -60°$.

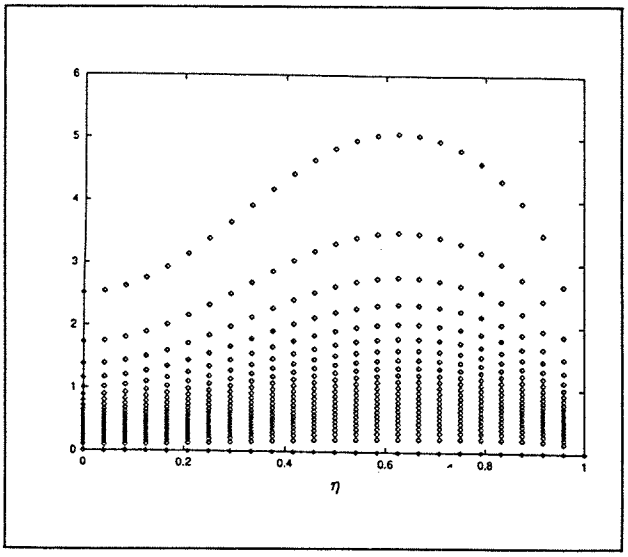

Figure 22: Spanwise Aerodynamic Load Distribution with $g_f = 0.$ and $g_t = 0.$ for $\Lambda = -60°$

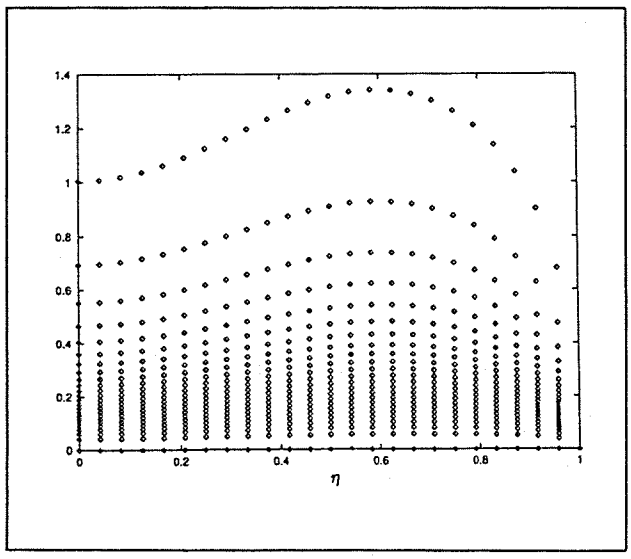

Figure 24: Spanwise Aerodynamic Load Distribution with $g_f = 0.5$ and $g_t = 0.5$ for $\Lambda = -60°$

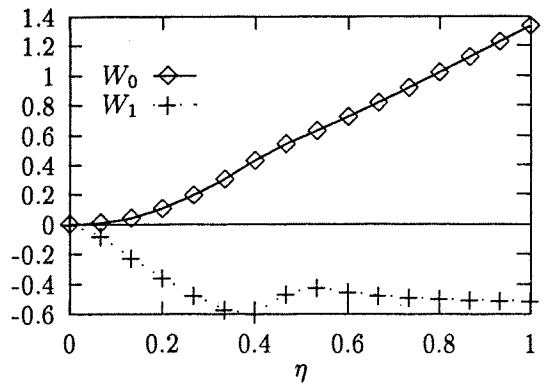

Figure 25: Center Line and Rotation Elastic Response to the Aerodynamic Load with $g_f = 1.$ and $g_t = 1.$ for $\Lambda = -60°$.

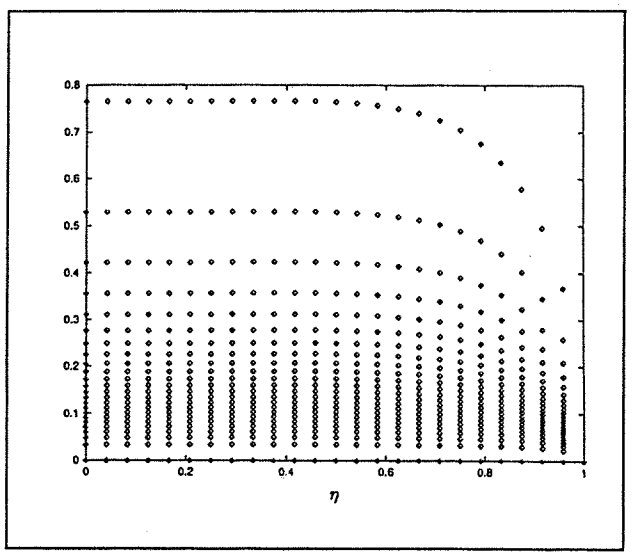

Figure 26: Spanwise Aerodynamic Load Distribution with $g_f = 1.$ and $g_t = 1.$ for $\Lambda = -60°$.